scientific reports

Check for updates

OPEN

Dynamic protected states in the non-Hermitian system

Lei Chen[1,2], Zhen-Xia Niu[3] & Xingran Xu[4]✉

The non-Hermitian skin effect and nonreciprocal behavior are sensitive to the boundary conditions, which are unique features of non-Hermitian systems. In such systems, eigenenergies can become complex, and all eigenstates tend to localize at the boundary, a phenomenon that contrasts with Hermitian topologies. In this work, we theoretically study the dynamic behavior of the propagation of Gaussian wavepackets inside a non-Hermitian lattice and analyze the self-acceleration process of bulk state or Gaussian wavepackets toward the system's boundary. The initial wavepackets will not only propagate toward the side where the eigenstates are localized, but also their momentum will approach to a specific value. This value corresponds to the maximum imaginary components of the energy dispersion. In addition, if the wavepackets in the momentum space cover this specific momentum, they will eventually exhibit exponentially increasing amplitudes with time evolution, maintaining the dynamic protected condition for an extended period of time until they approach the boundary. We also take two widely used toy models as examples in one and two dimensions to verify the correspondence of the non-Hermitian skin effect and the dynamic protected state.

Keywords Skin effect, Photonic lattice, Non-Hermitian Hamiltonian, Dynamic behavior

For an isolated quantum system, to ensure the conservation of energy and probability, a Hermitian Hamiltonian is necessary. When a quantum system couples to its environment, hence, particle loss and decoherence lead to the breakdown of Hermiticity and require non-Hermitian descriptions[1–5]. It has been shown that non-Hermitian considerations not only provide suitable descriptions of open systems, but also bring novel physics and unprecedented phenomena and applications, as found in a variety of physical realms including parity-time symmetry and spectral singularity[6–9], non-reciprocal and chiral transport[10], as well as non-Hermitian topology and unconventional band theory[11–14]. Within this context, particularly fascinating phenomenon is the recently discovered non-Hermitian skin effect (NHSE)[14–17].

The NHSE, an anomalous localization of extensive eigenstates at the open boundaries of a non-Hermitian system, is drastically different from the dynamics of the extended Bloch waves in Hermitian systems. This phenomenon was first discovered by Hatano and Nelson[18,19] in the late 1900s, where they proposed a one-dimension (1D) disordered tight-binding lattice model with nearest-neighbour nonreciprocal hopping and showed that non-Hermiticity induced by the nonreciprocity can prevent Anderson localization, opening up a mobility region characterized by unidirectional transportation. Recently, similar phenomena have also been observed in many seminal works on the topological properties of non-Hermitian systems. They either revisit the Hatano-Nelson (HN) model to realize versatile directional transports[20,21], interpret NHSE from different perspectives[22–27], even to develop new theories, methods, and material designs to describe NHSE related topological properties and the associated non-Hermitian bulk-boundary correspondence (BBC)[11,15,28–31], or extend NHSE to higher dimensions[32–35], to explore new NHSE features enriched by heterogeneous degrees of freedom[36–40], and experimentally demonstrating the NHSE[41–44].

One of the significant features of the NHSE is that the eigenstates are sensitive to the boundary conditions. The bulk properties of the open boundary condition (OBC) Hamiltonian can be well approximated by the Bloch Hamiltonian with periodic boundary conditions (PBCs), which is called the BBC in band theory[45]. However, the eigenstates with the NHSE cannot be characterized by the BBC because *all* of them are localized at the edge with OBCs in the finite-size sysytem[46–48]. In other words, the eigenstates and eigenenergies with the NHSE under different boundary conditions are completely different from each other. To solve this conflict, the generalized Brillouin zone (GBZ)[28,49,50] and biorthogonal BBC[15,51] have been proposed. GBZ theory takes the complex momentum and modifies the Bloch factor to obtain the OBC eigenenergies[11,14,15,52,53]. Therefore, the

[1]School of Information, Hunan University of Humanities, Science and Technology, Loudi 417000, China. [2]School of Physics and Electronic Science, Zunyi Normal University, Zunyi 563006, China. [3]Department of Physics, Zhejiang Normal University, Jinhua 321004, China. [4]School of Science, Jiangnan University, Wuxi 214122, China. ✉email: thoexxr@hotmail.com

corresponding eigenstates are exponentially localized at the edges of the system. Biorthogonal BBC theory uses both the left and right eigenstates to obtain the OBC eigenenergies from the PBC Hamiltonian. Moreover, the topological invariants of the system with the NHSE are also quite different. The winding number can be defined from the complex energy spectrum, where the complex energy spectrum under PBCs can form a loop and encircle all of the complex energy spectrum under OBCs[37,54].

The largest influence of the NHSE on the dynamic properties of the system is reflected in the appearance of a directional (chiral) bulk flow and persistent currents[23,25,55]. The wavefunctions inside the bulk have a nonreciprocal behavior where their propagation has a specific direction, which can be detected by experiments[56,57]. In addition, a novel bulk dynamic signature of the NHSE arises in the early stage of the time evolution, i.e., self acceleration of the wavefunction[57,58]. The complex energy spectrum of the eigenenergies will make the density of the wavepackets exhibit gain or loss for different momentums. The long time dynamics of the wavefunction are dominated by the interference of Bloch modes with the largest imaginary part of the energy, leading to a directional flow of excitation along the lattice at a constant drift velocity in systems, and displaying the NHSE. However, the imaginary parts of the eigenenergies can have more than one maximum (beyond zero), where the flow of condensates will have a competitive behavior between the maximum points of the eigenenergies.

In this work, we study the dynamic evolution of wavepackets with different velocities in non-Hermitian lattices. Our study reveals that wavepackets characterized by the maximum imaginary eigenenergies are dynamically protected by the bulk until they encounter the boundary. The paper is organized as follows. In "Finite size and the non-Hermitian skin effect" section, we introduce the simplest lattice with the NHSE and discuss the influence of the finite size on the energy spectrum and the localization of states. In "Dynamic protected state" section, we investigate the bulk protected states under OBCs and give the analytical result. In "Dynamic protected states of different non-Hermitian systems" section, we take two widely used models as examples to prove the universality in the non-Hermitian system. In "Discussion" section, we conclude with a summary of our main results and final remarks.

Finite size and the non-Hermitian skin effect

In this section, we review the influence of the size of the system with NHSE. The HN model is the simplest NHSE model, with

$$H=\sum_{n}\left(J_1C_{n+1}^{\dagger}C_n+J_2C_n^{\dagger}C_{n+1}\right), \tag{1}$$

where $C_n(C_n^{\dagger})$ is the annihilation (creation) operator at the n site index, J_1 and J_2 are the nearest-neighbor hopping energies along different directions.

The eigenenergies of the non-Hermitian skin Hamiltonian are always different with different boundary conditions. In particular, the periodic boundary eigenenergies can encircle all open boundary eigenenergies as shown in Fig. 1a, the HN model fundamentally gives purely real eigenenergies when the system has a small size L. However, when the system size increases, imaginary parts of the eigenenergies appear and approach the PBC result (blue signs in Fig. 1a). Based on this, the topological invariants can easily be defined[24,59] by

$$W=\frac{1}{2\pi i}\oint_C\frac{d}{dk}\log\left[Det\left(H(\hat{k})-E_R\hat{I}\right)\right], \tag{2}$$

where $H(k)=\sum_k\left[(J_1+J_2)\cos k-i(J_1-J_2)\sin k\right]C_k^{\dagger}C_k$ can be obtained by the Fourier transformation of the real-space Hamiltonian (see Fig. 1b) and E_R is the reference energy. The eigenenergies are complex when the system size is large enough or the system has PBCs. The winding number W is dependent on the sign of J_1-J_2. If $J_1=J_2$, the winding number is zero, all eigenenergies are real, and the NHSE vanishes. However, $J_1\neq J_2$ will let the topological invariants arise and all eigenstates localize at the side.

In the HN model, all wavefunctions are localized at the edge. The amplitudes of the absolute value of the density will exponentially increase or descrease (depending on the magnitude of J_1 and J_2) with the site index n, as illustrated in Fig. 1c. The relationship between the density of the first site and the last site can be described by

$$|\psi(n)|^2=e^{\kappa n}|\psi(1)|^2, \tag{3}$$

where κ is the scaling parameter and n is the site index. In a Hermitian lattice, the Bloch factor $|e^{ik}|=1$, however, GBZ theory states that $|e^{ik}|=\beta\neq 1$, where all wavefunctions can have exponential localization along the index. So the translation symmetry is broken in the non-Hermitian lattice[60,61] . As is illustrated in Fig. 1d, the scaling paramters κ is proportional to the inverse of the system size $\kappa\sim L^{-1}$. Therefore, the localization of the density will vanish when the system size goes to infinity.

Dynamic protected state

In this section, we will analyze the time evolution of the Gaussian wavepackets and obtain the motion of the center mass in the initial stage of evolution.

In a Hermitian topological system, only the edge states are topologically protected, and their propagation is chiral. However, all eigenstates of the non-Hermitian Hamiltonian are localized, including the bulk and edge states. The wavefunction is forbidden to propagate to one side and get enhanced to propagate to the opposite side in the 1D case[62,63].

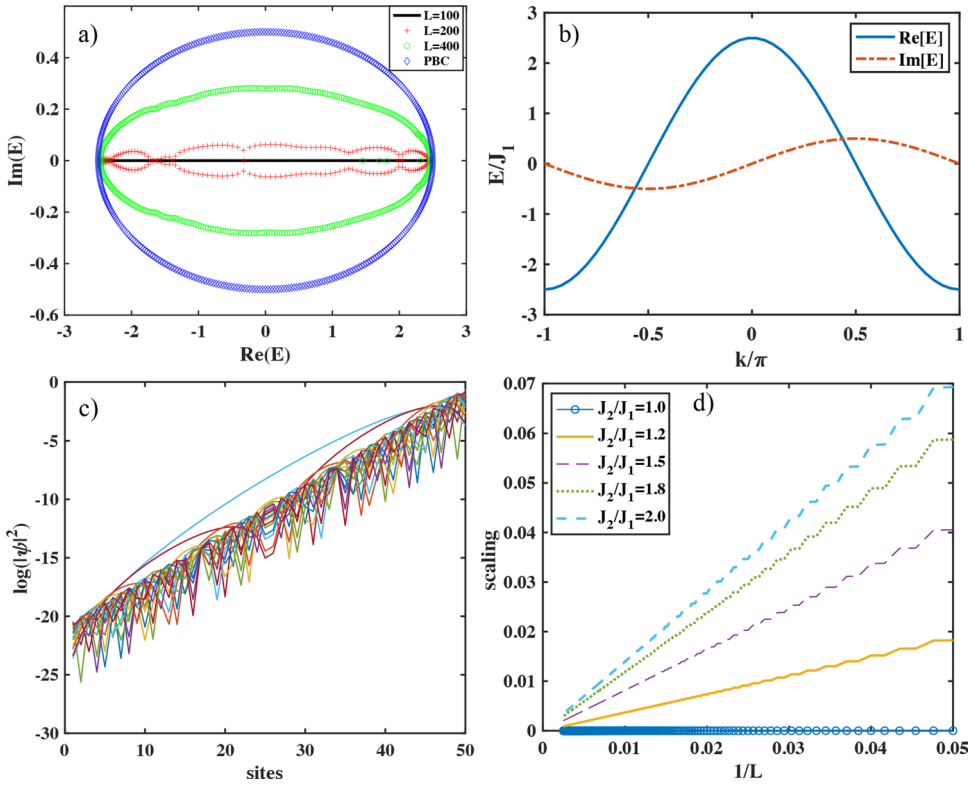


Fig. 1. (**a**) Complex energy spectrum of the HN model with different system sizes and (**b**) eigenenergies with PBCs. (**c**) Log function of the density of the eigenstates, and (**d**) the scaling parameter κ as a function of the system size L in Eq. (3). We take $J_1 = 1$ and $J_2/J_1 = 1.5$ for (**a**), (**b**) and (**c**).

When we consider the time evolution of the wavepackets of the system, we need to expand the initial state with the eigenstates. The eigenenergies are complex for a non-Hermitian system with PBCs or a sufficiently large size. The wavepacket with momentum k evolutes with time as follows,

$$|\psi(k,t)\rangle = e^{-iRe(E)t}e^{Im(E)t}|\psi(k,0)\rangle, \tag{4}$$

where the real eigenenergies ($Re\ (E)$) govern the motion of the wavepacket and the imaginary eigenenergies describe the decay or growth rate of the corresponding eigenstates. When $Im(E) < 0$ or $Im(E) > 0$, the corresponding eigenstate will exponentially decay or grow with time. Therefore, the time evolution of the wavefunction will have a peculiar dynamic behavior where all wavefunctions in momentum space will become the same.

The time evolution of the wavefunction in momentum space can be obtained by the Fourier transformation, with

$$\psi(k,0) = \sum_{n=0}^{L-1} \psi(n,0)e^{-ikn}. \tag{5}$$

As shown in Fig. 2, we place the Gaussian state with different initial velocities k_0 in the center of the HN lattice . The wavepacket has nonreciprocal behavior, and its center of mass only moves to one side. In addition, if the initial momentum is not equal to the momentum $k_m = \pi/2$ where the imaginary eigenenergies have the maximum, then the momentum of the wavepacket will approach k_m. Specifically, when we use $k_0 = k_m$ as the momentum of the initial state, the Gaussian state is protected until it reaches the boundary which is unique compared to the Hermitian topological lattice. Due to the maximum of the imaginary energies in the non-Hermitian lattice with PBCs, only the wavefunction with momentum k_m will be the most enhanced along with the time evolution. Therefore, the propagation of the wavepacket with OBCs in the bulk can still obey the rule of PBCs and survive for a sufficiently long time until it reaches the boundary.

The duration of the wavepacket with OBCs linearly increases with the system size, as illustrated in Fig. 3. When we set the momentum of the initial state near k_m ($k_0 = 0.4\pi$), the speed of wavepacket $k(t)$ will keep a duration at k_m, and then maintain a long time unless reaching the boundary. The initial state in momentum space can be described as

$$\psi(k,0) = e^{(k-k_0)^2/2\sigma^2}, \tag{6}$$

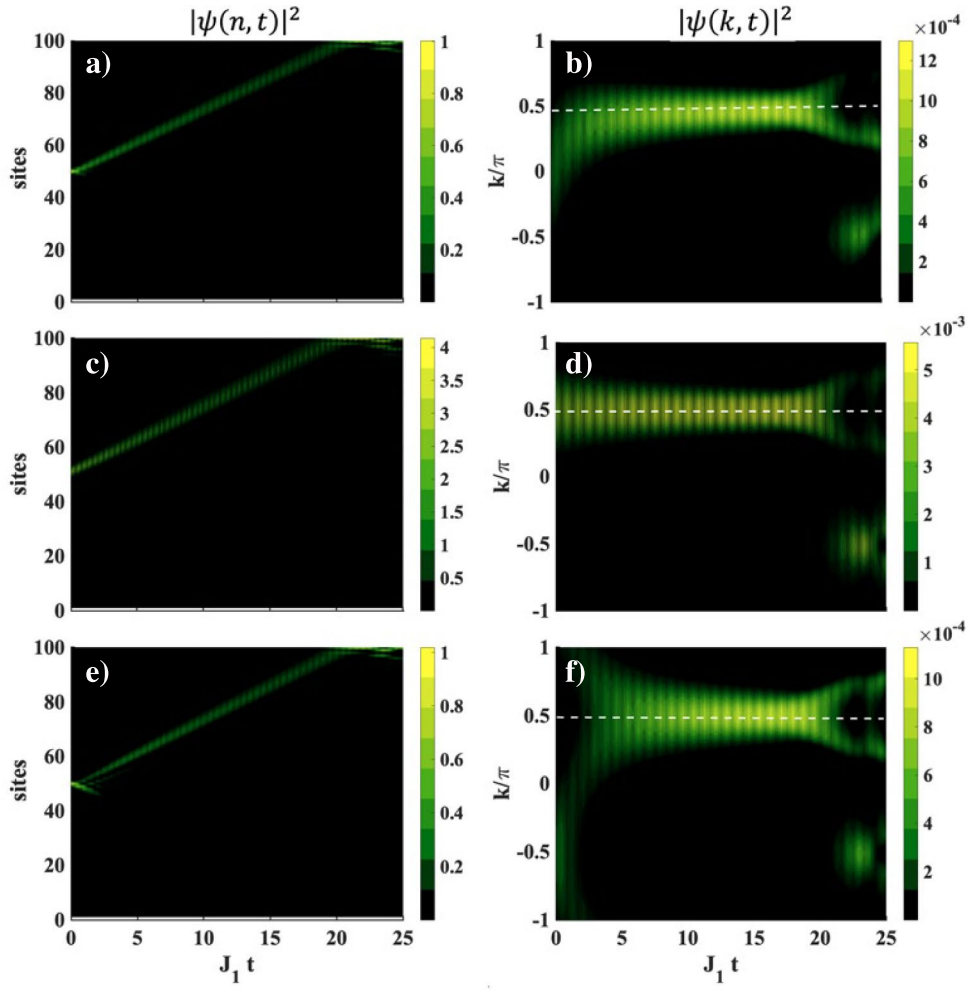


Fig. 2. Time evolution of the Gaussian wavepackets with different initial momenta in real space (first column) and momentum space (second column). The parameters are $J_2/J_1 = 1.5$, $k_0 = 0$, and $-\pi/2$ or $\pi/2$ for different rows.

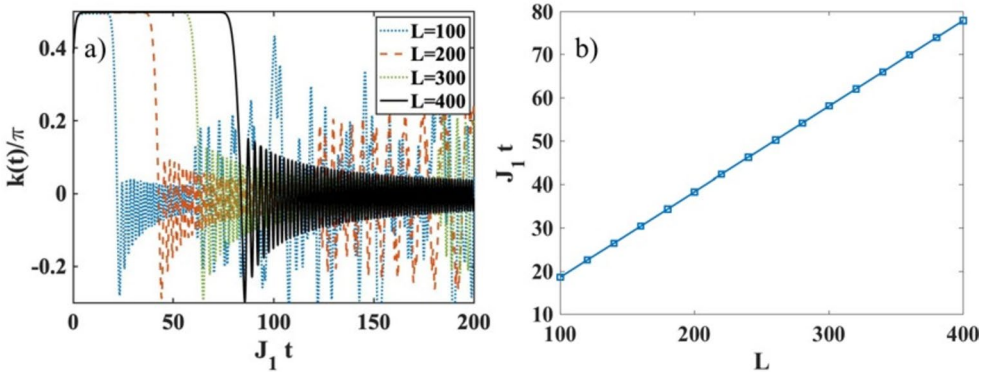


Fig. 3. The mean momentums of the wavepackets changes with time at different system sizes L (**a**), and the duration of the dynamic protected state as a function of the system size (**b**). Parameters are $J_2/J_1 = 1.5$ and $k_0 = 0.4\pi$.

where k_0 is the center of the wavepacket in k space and σ is the width. When the Gaussian state is in the bulk, we can use the PBC Hamiltonian to explain the wavepacket dynamic properties, with

$$\psi(k,t) = e^{-it\sum_k (J_1+J_2)\cos k-(J_1-J_2)\sin k} e^{(k-k_0)^2/2\sigma^2}. \tag{7}$$

The first term is the oscillation frequency and can be ignored compared to the exponential decay or gain due to the imaginary eigenenergies.

We consider a non-Hermitian Hamiltonian, denoted as $\hat{H} = \sum_k E_k|k\rangle\langle k|$, where $|k\rangle$ represents the right eigenvector with eigenenergy E_k. An initial state $|\psi(t=0)\rangle$ is governed by the evolution operator $U(t)$ associated with this Hamiltonian. The state at time t, denoted as $|\psi(k,t)\rangle$, is determined by the evolution operator $U(t)$ associated with the Hamiltonian. Mathematically, it can be expressed as

$$\begin{aligned} |\psi(k,t)\rangle =& \hat{U}(t)|\psi(k,0)\rangle = e^{-i\hat{H}t}|\psi(k,0)\rangle \\ =& \prod_k e^{-iE_k t|k\rangle\langle k|}|\psi(k,0)\rangle. \end{aligned} \tag{8}$$

Let us examine the variation in the mean momentum over time, given by $\langle\psi(k,t)|\hat{k}|\psi(k,t)\rangle$.

$$\begin{aligned} k(t) =& \langle\psi(k,t)|\hat{k}|\psi(k,t)\rangle \\ =& \langle\psi(k,0)|\prod_{k_2} e^{iE^*_{k_2}t|k_2\rangle\langle k_2|}\hat{k}\prod_{k_1} e^{-iE_{k_1}t|k_1\rangle\langle k_1|}|\psi(k,0)\rangle \\ =& \int dk'\langle\psi(k,0)|k'\rangle e^{i(E^*_{k'}-E_{k'})t}k'\langle k'|\psi(k,0)\rangle \\ =& \int dk' e^{2ImE_{k'}t}k'|\langle k'|\psi(k,0)\rangle|^2, \end{aligned} \tag{9}$$

where we insert a unit operator $\int dk'|k'\rangle\langle k'|$. In Hermitian systems, $E_{k'}$ is purely real, observing that $k(t) = k(0)$ remains unchanged with time evolution. In non-Hermitian systems, when $Im(E_{k'}) > 0$, the contribution of k' becomes more significant, while $Im(E_{k'}) < 0$, the contribution of k' diminishes. A predictable consequence is that $k(t)$ eventually approaches k_m, which corresponds to the maximum value of $Im(E_{k_m})$. Without loss of generality, we can shift $Im(E_k)$ such that the maximum point corresponds to zero. We can obtain

$$k(t) = \int dk' e^{2Im(\tilde{E}_{k'})t}e^{2at}k'|\langle k'|\psi(k,0)\rangle|^2, \tag{10}$$

where $Im(\tilde{E}_{k'}) = Im(E_{k'} - a)$, where a is a positive constant. We consider a simplified case where $a = 0$, indicating that only dissipative effects are present in the system. The contribution of all values of k except for the maximum point decreases. Therefore, as long as $|\langle k_m|\psi(0)\rangle|^2$ is nonzero, $\lim_{t\to\infty} k(t)$ remains equal to k_m.

Therefore, the dynamic protected states are the wavepacket that will not change with time during the propagation period. The momentum of the wavepackets will approach to the k_m, which is the maximum point of the imaginary parts of the eigenenergies of the non-Hermitian Hamiltonian with NHSE.

Dynamic protected states of different non-Hermitian systems

In this section, we take two widely used theoretical models (the SSH model and 2D polariton system) with different symmetries as examples to check the universality of the dynamic protected state in non-Hermitian systems and discuss the influence of the skin effect. The time and energy dimensions are normalized with $J_1 t$ and E/J_1.

SSH model with chiral symmetry

The SSH model with different nearest-neighbor hopping energies in a 1D lattice is widely studied to realize the NHSE[64,65]. The Hamiltonian in momentum k space can be described as

$$H = d_x\sigma_x + (d_y + i\frac{\gamma}{2})\sigma_y, \tag{11}$$

where $\gamma/2$ changes the hopping term in the unit cell with different hopping strengths. $d_x = t_1 + t_2\cos k$, $d_y = t_2\sin k$ and $\sigma_{x,y}$ are the Pauli matrices. t_1 and t_2 are the hopping between the different spins in the same unit cell and the hopping between the nearest unit cells.

The real parts and imaginary parts of eigenvalues of Eq. (11) with the Fourier transformation in momentum space are shown in Fig. 4a,b. All eigenstates with OBCs are localized at the left side (shown in Fig. 4c) when $t_1 < t_2$. The eigenvalues appear in pairs, with

$$E_\pm(k) = \pm\sqrt{t_1^2 + t_2^2 + 2t_1t_2\cos k - \gamma^2/4 + it_2\gamma\sin k}. \tag{12}$$

The OBC eigenenergies are zero modes in the finite-size system, and GBZ theory gives the non-Bloch factor $|e^{ik}| = \sqrt{\left|\frac{t_1-\gamma/2}{t_1+\gamma/2}\right|} \neq 1$, where k becomes a complex number and makes the eigenstates localized.

The imaginary parts of eigenvalues of different spins have different maximum points k_m and $-k_m$ (red solid line and blue dashed line in Fig. 4b) with PBC. When we place the initial Gaussian state in the middle of the

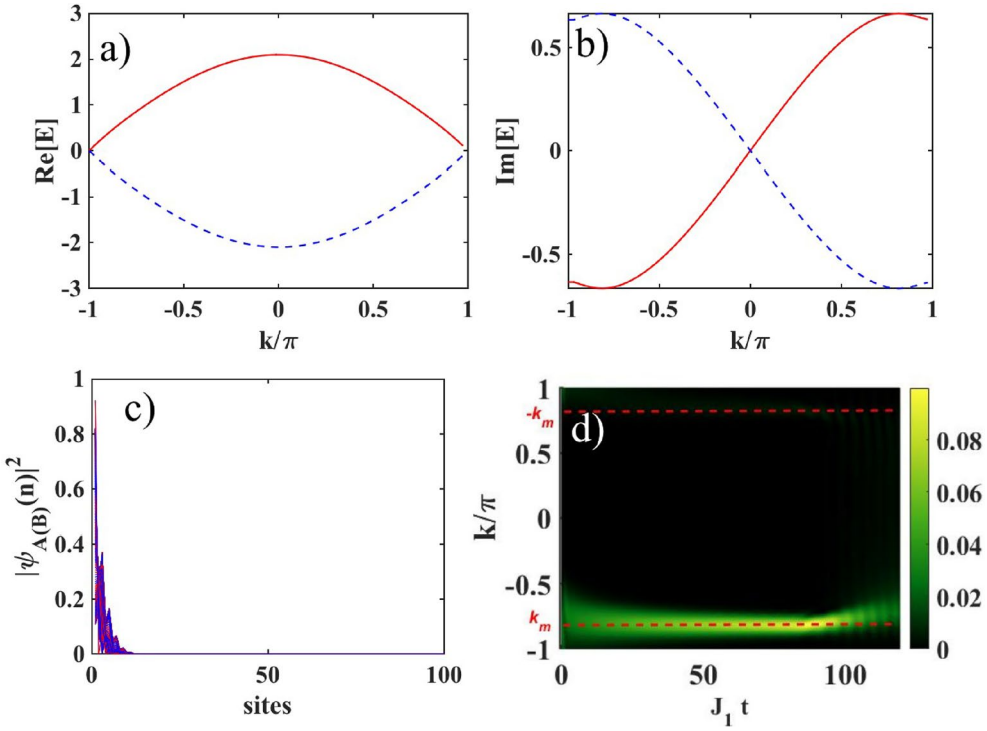


Fig. 4. The real (**a**) and the imaginary (**b**) parts of the eigenenergies of the SSH model with different spins. Eigenfunctions of different spins (**c**), and the density evolution of spin-up with the initial velocity $k_0 = -0.5\pi$ (**d**). The other parameters are $t_2/t_1 = 1.2$ and $\gamma/t_1 = 4/3$.

lattice with OBC, the mean momentum of the wavepacket will have two peaks k_m and $-k_m$. However, the density of $|\psi(k,t)|^2$ are most localized at k_m rather than $-k_m$ as shown in Fig. 4d. The above results imply that the boundary condition plays a significant role in the non-Hermitian system with skin effect. The eigenstates of the Hamiltonian with OBC are localized at the left side (shown in Fig. 4c), so dynamic behaviors of a condensation in the bulk are also affected by the boundary condition and propagate to the left side with momentum k_m.

Two-dimensional non-Hermitian system

In this subsection we will discuss dynamic behaviors and preotected states of the higher-order NHSE in 2D polariton system. The previous work[54] have revealed that all wavefunctions are localized at the corners in 2D tight-binding polariton model. The effective Hamiltonian can be described as

$$\begin{aligned} H_{m,n} = &\sum_{m,n}\left[J_1\left(\hat{a}^\dagger_{m,n}\hat{a}_{m,n+1} + \hat{b}^\dagger_{m,n}\hat{b}_{m,n+1} + h.c.\right) + J_2\left(\hat{a}^\dagger_{m+1,n}\hat{a}_{m,n} + \hat{b}^\dagger_{m+1,n}\hat{b}_{m,n} + h.c.\right)\right] \\ &+ \sum_{m,n}\left[-i\gamma_+\left(\hat{a}^\dagger_{m,n}\hat{a}_{m,n}\right) - i\gamma_-\left(\hat{b}^\dagger_{m,n}\hat{b}_{m,n}\right)\right] \\ &+ \sum_{m,n}\left[A\hat{a}^\dagger_{m,n}\hat{b}_{m,n}e^{-ik_p(m+n)} + A\hat{b}^\dagger_{m,n}\hat{a}_{m,n}e^{ik_p(m+n)}\right], \end{aligned} \tag{13}$$

where $\hat{a}_{m,n}$ ($\hat{a}^\dagger_{m,n}$) and $\hat{b}_{m,n}$ ($\hat{b}^\dagger_{m,n}$) denote the annihilation (creation)of particles with spin ± at site (m, n). $J_{1,2}$ are the hopping energies in the x and y directions, $\gamma_\pm$ are the different decay (or gain) rates of different spins, and A describes the strength of the polarization splitting.

As shown in Fig. 5a, the eigenenergies with OBC (black dots) are surrounded by the PBC energies (green and blue areas). All wavefunctions are localized at the off-side corners and the winding number is dependent on the selected paths. Furthermore, only along with the path $k_x = k_y$ (red circles), all OBC eigenenergies are encircled by the PBC eigenenergies in this path[54]. The eigenenergies of different spins are plotted with different colors (green and blue areas) and they are separated from each other. The winding number for each spin is opposite and their corresponding eigenstates are localized at the opposite corners[54]. The system can be transformed into a two-band model with PBC and the real and imaginary parts of the corresponding eigenenergies as shown in Fig. 5b and c. The real parts are separated from each other, but the imaginary parts have crossovers. The higer order NHSE is different from the 1D case since the winding number is determined by the chosen integrated path.

The imaginary parts of the eigenenergies of Eq. (13) have multiple maximum points as illustrated in Fig. 5c. To check the density distrubution in the momentum space, we place two Gaussian states with zero initial speeds at the middle of the lattice in Fig. 6. The density distribution of two spins will gain velocities because of the

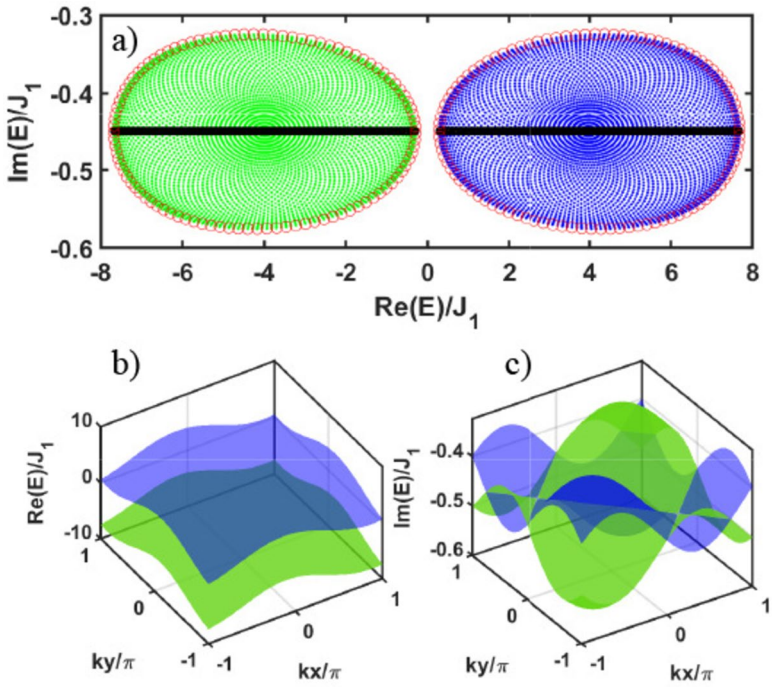


Fig. 5. Complex energy spectrum with PBCs and OBCs (**a**), and real (**b**) and imaginary (**c**) energy bands of PBC eigenenergies. The black lines are the OBC energies, and the blue and green areas are filled with the PBC energies of the upper and lower bands. Meanwhile, the green dots are the complex energies along with the selected integration direction for defining the winding number in (**a**). Parameters: $J_2/J_1 = 1$, $k_p = \pi/4$, $\gamma_+/J_1 = 0.1$, $\gamma_-/J_1 = 0.8$, and $A/J_1 = 4$.

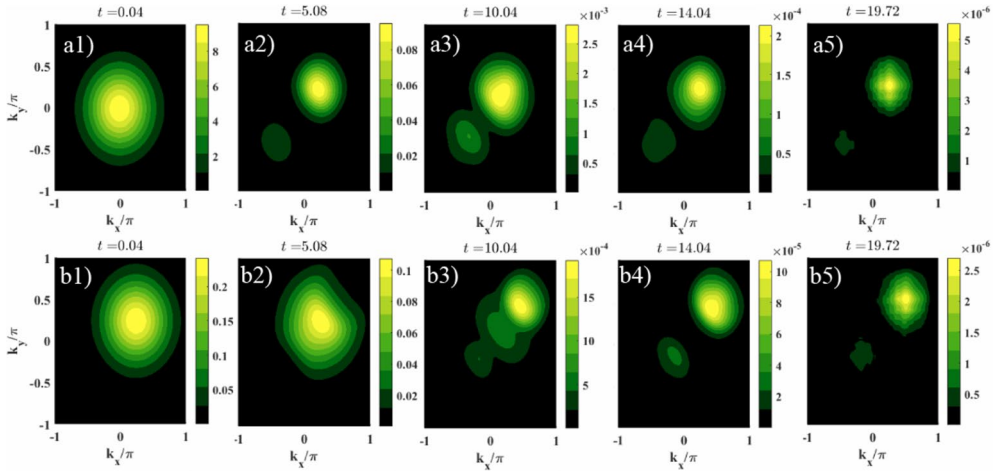


Fig. 6. Time evolution of the Gaussian states in momentum space for different spins (different rows) obtained with Hamiltonian Eq. (13). Parameters: $J_2/J_1 = 1$, $k_p = \pi/4$, $\gamma_+/J_1 = 0.1$, $\gamma_-/J_1 = 0.8$, and $A/J_1 = 4$.

self-accelaration effect[55]. However, all eigenstates of the OBC Hamiltonian are localized at the off-side corners. Here, the effective decays for different spins $\gamma_\pm$ have the crucial effect for letting the density decay along with different directions are different in the time evolution.

At the begining, the density distribution for different spins in momentum space are localized at the different k_x and k_y as shown in Fig. 6a1,a2 and b1,b2. After the sufficient long time, the two-dimensional Gaussian states in momentum space will remain stable as shown in Fig. 6a3–a5 and b3–b5. In addition, the density distributions for different spins are localized at the same k_x and k_y although the imaginary parts of the eigenenergies of the PBC Hamiltonian are different and have different maximum points. The eigenstates of the non-Hermitian system are sensitive to the boundary condition and so do the dynamic protected states.

Discussion

In this work, we study the time evolution of the wavepackets in a non-Hermitian lattice. The wavepackets are initialized as Gaussian states, each characterized by distinct center-of-mass positions and initial velocities. Intriguingly, the mean momentum of these Gaussian wavepackets tends to align with a specific momentum value, where the system's eigenenergies exhibit the most significant imaginary components. This alignment results in a dynamically protected state that remains stable within the bulk under open boundary conditions (OBC), initiating an exponential acceleration from the initial velocity. This state maintains its momentum over an extended period, persisting until the wavepackets encounter the lattice boundaries. We further illustrate our findings using the one-dimensional SSH model and a two-dimensional polariton system, both of which feature eigenenergies with multiple maxima. The momentum of the Gaussian wavepackets is found to be influenced by the localization of eigenstates on either side of the lattice and is sensitive to the boundary conditions.

Our findings not only enhance the understanding of the non-Hermitian skin effect and the self-acceleration of wavefunctions but also highlight the sensitivity and robustness of bulk state evolution across different momenta within non-Hermitian lattices. These insights are crucial for the development of novel quantum devices, such as making the electronic sensor with a high-level sensitivity and a strong robustness[66,67], advancing non-Hermitian topological magnonics and photonics to deal with the engineering of dissipation and/or gain for non-Hermitian topological phases[68–70], opening new avenues for innovative applications[71,72].

Data availability

The datasets used and analysed during the current study are available from the corresponding author on reasonable request.

Received: 17 May 2024; Accepted: 9 September 2024
Published online: 18 September 2024

References

1. Carmichael, H. J. Quantum trajectory theory for cascaded open systems. *Phys. Rev. Lett.* **70**(15), 2273. https://doi.org/10.1103/physrevlett.70.2273 (1993).
2. Bender, C. M. & Boettcher, S. Real spectra in non-Hermitian Hamiltonians having PT symmetry. *Phys. Rev. Lett.* **80**, 5243–5246. https://doi.org/10.1103/PhysRevLett.80.5243 (1998).
3. Bender, C. M., Boettcher, S. & Meisinger, P. N. Pt-symmetric quantum mechanics. *J. Math. Phys.* **40**(5), 2201–2229. https://doi.org/10.1063/1.532860 (1999).
4. Bender, C. M., Brody, D. C. & Jones, H. F. Complex extension of quantum mechanics. *Phys. Rev. Lett.* **89**(27), 270401. https://doi.org/10.1103/physrevlett.89.270401 (2002).
5. Ashida, Y., Gong, Z. & Ueda, M. Non-Hermitian physics. *Adv. Phys.* **69**(3), 249–435. https://doi.org/10.1080/00018732.2021.1876991 (2020).
6. Bender, C. M. Making sense of non-Hermitian Hamiltonians. *Rep. Prog. Phys.* **70**(6), 947. https://doi.org/10.1088/0034-4885/70/6/r03 (2007).
7. El-Ganainy, R. *et al.* Non-Hermitian physics and PT symmetry. *Nat. Phys.* **14**(1), 11–19. https://doi.org/10.1038/nphys4323 (2018).
8. Özdemir, ŞK., Rotter, S., Nori, F. & Yang, L. Parity-time symmetry and exceptional points in photonics. *Nat. Mater.* **18**(8), 783–798. https://doi.org/10.1038/s41563-019-0304-9 (2019).
9. Miri, M.-A. & Alu, A. Exceptional points in optics and photonics. *Science* **363**(6422), 7709. https://doi.org/10.1126/science.aar7709 (2019).
10. Fruchart, M., Hanai, R., Littlewood, P. B. & Vitelli, V. Non-reciprocal phase transitions. *Nature* **592**(7854), 363–369. https://doi.org/10.1038/s41586-021-03375-9 (2021).
11. Kawabata, K., Shiozaki, K., Ueda, M. & Sato, M. Symmetry and topology in non-Hermitian physics. *Phys. Rev. X* **9**, 041015. https://doi.org/10.1103/PhysRevX.9.041015 (2019).
12. Zhou, H. & Lee, J. Y. Periodic table for topological bands with non-Hermitian symmetries. *Phys. Rev. B* **99**, 235112. https://doi.org/10.1103/PhysRevB.99.235112 (2019).
13. Yokomizo, K. & Murakami, S. Non-bloch band theory of non-Hermitian systems. *Phys. Rev. Lett.* **123**, 066404. https://doi.org/10.1103/PhysRevLett.123.066404 (2019).
14. Yao, S. & Wang, Z. Edge states and topological invariants of non-Hermitian systems. *Phys. Rev. Lett.* **121**, 086803. https://doi.org/10.1103/PhysRevLett.121.086803 (2018).
15. Kunst, F. K., Edvardsson, E., Budich, J. C. & Bergholtz, E. J. Biorthogonal bulk-boundary correspondence in non-Hermitian systems. *Phys. Rev. Lett.* **121**, 026808. https://doi.org/10.1103/PhysRevLett.121.026808 (2018).
16. Lee, C. H. & Thomale, R. Anatomy of skin modes and topology in non-Hermitian systems. *Phys. Rev. B* **99**, 201103. https://doi.org/10.1103/PhysRevB.99.201103 (2019).
17. McDonald, A., Pereg-Barnea, T. & Clerk, A. Phase-dependent chiral transport and effective non-Hermitian dynamics in a bosonic Kitaev-Majorana chain. *Phys. Rev. X* **8**(4), 041031. https://doi.org/10.1103/physrevx.8.041031 (2018).
18. Hatano, N. & Nelson, D. R. Localization transitions in non-Hermitian quantum mechanics. *Phys. Rev. Lett.* **77**, 570–573. https://doi.org/10.1103/PhysRevLett.77.570 (1996).
19. Hatano, N. & Nelson, D. R. Vortex pinning and non-Hermitian quantum mechanics. *Phys. Rev. B* **56**, 8651–8673. https://doi.org/10.1103/PhysRevB.56.8651 (1997).
20. Longhi, S., Gatti, D. & Valle, G. D. Robust light transport in non-Hermitian photonic lattices. *Sci. Rep.* **5**(1), 13376. https://doi.org/10.1038/srep13376 (2015).
21. Longhi, S., Gatti, D. & Della Valle, G. Non-Hermitian transparency and one-way transport in low-dimensional lattices by an imaginary gauge field. *Phys. Rev. B* **92**(9), 094204. https://doi.org/10.1103/physrevb.92.094204 (2015).
22. Martinez Alvarez, V., Barrios Vargas, J. & Foa Torres, L. Non-Hermitian robust edge states in one dimension: Anomalous localization and eigenspace condensation at exceptional points. *Phys. Rev. B* **97**(12), 121401. https://doi.org/10.1103/physrevb.97.121401 (2018).
23. Zhang, K., Yang, Z. & Fang, C. Correspondence between winding numbers and skin modes in non-Hermitian systems. *Phys. Rev. Lett.* **125**, 126402. https://doi.org/10.1103/PhysRevLett.125.126402 (2020).
24. Okuma, N., Kawabata, K., Shiozaki, K. & Sato, M. Topological origin of non-Hermitian skin effects. *Phys. Rev. Lett.* **124**, 086801. https://doi.org/10.1103/PhysRevLett.124.086801 (2020).
25. Longhi, S. Probing non-Hermitian skin effect and non-bloch phase transitions. *Phys. Rev. Research* **1**, 023013. https://doi.org/10.1103/PhysRevResearch.1.023013 (2019).

26. Song, F., Yao, S. & Wang, Z. Non-Hermitian skin effect and chiral damping in open quantum systems. *Phys. Rev. Lett.* **123**, 170401. https://doi.org/10.1103/PhysRevLett.123.170401 (2019).
27. Yokomizo, K. & Murakami, S. Scaling rule for the critical non-Hermitian skin effect. *Phys. Rev. B* **104**(16), 165117. https://doi.org/10.1103/physrevb.104.165117 (2021).
28. Yang, Z., Zhang, K., Fang, C. & Hu, J. Non-Hermitian bulk-boundary correspondence and auxiliary generalized brillouin zone theory. *Phys. Rev. Lett.* **125**, 226402. https://doi.org/10.1103/PhysRevLett.125.226402 (2020).
29. Xu, K. *et al.* Coexistence of topological edge states and skin effects in the non-Hermitian Su-Schrieffer-Heeger model with long-range nonreciprocal hopping in topoelectric realizations. *Phys. Rev. B* **103**(12), 125411. https://doi.org/10.1103/physrevb.103.125411 (2021).
30. Claes, J. & Hughes, T. L. Skin effect and winding number in disordered non-Hermitian systems. *Phys. Rev. B* **103**(14), 140201. https://doi.org/10.1103/physrevb.103.l140201 (2021).
31. Okuma, N. & Sato, M. Non-Hermitian skin effects in Hermitian correlated or disordered systems: Quantities sensitive or insensitive to boundary effects and pseudo-quantum-number. *Phys. Rev. Lett.* **126**(17), 176601. https://doi.org/10.1103/physrevlett.126.176601 (2021).
32. Yao, S., Song, F. & Wang, Z. Non-Hermitian chern bands. *Phys. Rev. Lett.* **121**, 136802. https://doi.org/10.1103/PhysRevLett.121.136802 (2018).
33. Fu, Y., Hu, J. & Wan, S. Non-Hermitian second-order skin and topological modes. *Phys. Rev. B* **103**, 045420. https://doi.org/10.1103/PhysRevB.103.045420 (2021).
34. Kim, K.-M. & Park, M. J. Disorder-driven phase transition in the second-order non-Hermitian skin effect. *Phys. Rev. B* **104**(12), 121101. https://doi.org/10.1103/physrevb.104.l121101 (2021).
35. Ghorashi, S. A. A., Li, T., Sato, M. & Hughes, T. L. Non-Hermitian higher-order Dirac semimetals. *Phys. Rev. B* **104**(16), 161116. https://doi.org/10.1103/physrevb.104.l161116 (2021).
36. Okuma, N. & Sato, M. Topological phase transition driven by infinitesimal instability: Majorana fermions in non-Hermitian spintronics. *Phys. Rev. Lett.* **123**, 097701. https://doi.org/10.1103/PhysRevLett.123.097701 (2019).
37. Xu, X. *et al.* Interaction-induced double-sided skin effect in an exciton-polariton system. *Phys. Rev. B* **103**, 235306. https://doi.org/10.1103/PhysRevB.103.235306 (2021).
38. Lin, Z., Ding, L., Ke, S. & Li, X. Steering non-Hermitian skin modes by synthetic gauge fields in optical ring resonators. *Opt. Lett.* **46**(15), 3512. https://doi.org/10.1364/OL.431904 (2021).
39. Sun, X.-Q., Zhu, P. & Hughes, T. L. Geometric response and disclination-induced skin effects in non-Hermitian systems. *Phys. Rev. Lett.* **127**(6), 066401. https://doi.org/10.1103/physrevlett.127.066401 (2021).
40. Yuce, C. Nonlinear non-Hermitian skin effect. *Phys. Lett. A* **408**, 127484. https://doi.org/10.1016/j.physleta.2021.127484 (2021).
41. Zhang, K., Yang, Z. & Fang, C. Universal non-Hermitian skin effect in two and higher dimensions (2021)
42. Zhang, L. *et al.* Acoustic non-Hermitian skin effect from twisted winding topology (2021)
43. Liang, Q. *et al.* Dynamic signatures of non-Hermitian skin effect and topology in ultracold atoms. *Phys. Rev. Lett.* **129**(7), 070401. https://doi.org/10.1103/physrevlett.129.070401 (2022).
44. Shang, C. *et al.* Experimental identification of the second-order non-Hermitian skin effect with physics-graph-informed machine learning. *Adv. Sci.* **9**(36), 2202922. https://doi.org/10.1002/advs.202202922 (2022).
45. Alase, A., Cobanera, E., Ortiz, G. & Viola, L. Exact solution of quadratic fermionic Hamiltonians for arbitrary boundary conditions. *Phys. Rev. Lett.* **117**, 076804. https://doi.org/10.1103/PhysRevLett.117.076804 (2016).
46. Helbig, T. *et al.* Generalized bulk–boundary correspondence in non-Hermitian topolectrical circuits. *Nat. Phys.* **16**(7), 747–750. https://doi.org/10.1038/s41567-020-0922-9 (2020).
47. Liu, C.-H., Zhang, K., Yang, Z. & Chen, S. Helical damping and dynamical critical skin effect in open quantum systems. *Phys. Rev. Res.* **2**, 043167. https://doi.org/10.1103/PhysRevResearch.2.043167 (2020).
48. Lee, C. H., Li, L. & Gong, J. Hybrid higher-order skin-topological modes in nonreciprocal systems. *Phys. Rev. Lett.* **123**, 016805. https://doi.org/10.1103/PhysRevLett.123.016805 (2019).
49. Xiao, L. *et al.* Non-Hermitian bulk–boundary correspondence in quantum dynamics. *Nat. Phys.* **16**(7), 761–766. https://doi.org/10.1038/s41567-020-0836-6 (2020).
50. Imura, K.-I. & Takane, Y. Generalized bulk-edge correspondence for non-Hermitian topological systems. *Phys. Rev. B* **100**, 165430. https://doi.org/10.1103/PhysRevB.100.165430 (2019).
51. Xu, X., Liu, H., Zhang, Z. & Liang, Z. The non-Hermitian geometrical property of 1D Lieb lattice under Majorana's stellar representation. *J. Phys-Condens. Mat.* **32**(42), 425402. https://doi.org/10.1088/1361-648x/ab9fd4 (2020).
52. Gong, Z. *et al.* Topological phases of non-Hermitian systems. *Phys. Rev. X* **8**, 031079. https://doi.org/10.1103/PhysRevX.8.031079 (2018).
53. Lieu, S. Topological phases in the non-Hermitian Su-Schrieffer-Heeger model. *Phys. Rev. B* **97**, 045106. https://doi.org/10.1103/PhysRevB.97.045106 (2018).
54. Xu, X., Bao, R. & Liew, T. C. H. Non-Hermitian topological exciton-polariton corner modes. *Phys. Rev. B* **106**, 201302. https://doi.org/10.1103/PhysRevB.106.L201302 (2022).
55. Longhi, S. Non-Hermitian skin effect and self-acceleration. *Phys. Rev. B* **105**, 245143. https://doi.org/10.1103/PhysRevB.105.245143 (2022).
56. Weidemann, S., Kremer, M., Longhi, S. & Szameit, A. Topological triple phase transition in non-Hermitian floquet quasicrystals. *Nature* **601**(7893), 354–359. https://doi.org/10.1038/s41586-021-04253-0 (2022).
57. Lin, Q. *et al.* Topological phase transitions and mobility edges in non-Hermitian quasicrystals. *Phys. Rev. Lett.* **129**, 113601. https://doi.org/10.1103/PhysRevLett.129.113601 (2022).
58. Parto, M., Leefmans, C., Williams, J., Nori, F. & Marandi, A. Non-abelian effects in dissipative photonic topological lattices. *Nat. Commun.*[SPACE]https://doi.org/10.1038/s41467-023-37065-z (2023).
59. Zhang, X., Zhang, T., Lu, M.-H. & Chen, Y.-F. A review on non-Hermitian skin effect. *Adv. Phys. X*[SPACE]https://doi.org/10.1080/23746149.2022.2109431 (2022).
60. Wang, Y.-C., Jen, H. H. & You, J.-S. Scaling laws for non-Hermitian skin effect with long-range couplings. *Phys. Rev. B* **108**, 085418. https://doi.org/10.1103/PhysRevB.108.085418 (2023).
61. Qin, F., Ma, Y., Shen, R. & Lee, C. H. Universal competitive spectral scaling from the critical non-Hermitian skin effect. *Phys. Rev. B* **107**, 155430. https://doi.org/10.1103/PhysRevB.107.155430 (2023).
62. Hu, Y.-M.R., Ostrovskaya, E. A. & Estrecho, E. Wave-packet dynamics in a non-Hermitian exciton-polariton system. *Phys. Rev. B* **108**, 115404. https://doi.org/10.1103/PhysRevB.108.115404 (2023).
63. Malzard, S., Cancellieri, E. & Schomerus, H. Topological dynamics and excitations in lasers and condensates with saturable gain or loss. *Opt. Express* **26**(17), 22506. https://doi.org/10.1364/OE.26.022506 (2018).
64. Liu, J. S., Han, Y. Z. & Liu, C. S. A new way to construct topological invariants of non-Hermitian systems with the non-Hermitian skin effect. *Chin. Phys. B* **29**(1), 010302. https://doi.org/10.1088/1674-1056/ab5937 (2020).
65. Fu, Z. *et al.* Extended SSH model in non-Hermitian waveguides with alternating real and imaginary couplings. *Appl. Sci.* **10**(10), 3425. https://doi.org/10.3390/app10103425 (2020).
66. Yuan, H. *et al.* Non-Hermitian topolectrical circuit sensor with high sensitivity. *Adv. Sci.*[SPACE]https://doi.org/10.1002/advs.202301128 (2023).

67. Zhang, X. *et al.* Observation of continuum landau modes in non-Hermitian electric circuits. *Nat. Commun.*[SPACE]https://doi.org/10.1038/s41467-024-46122-0 (2024).
68. Yu, T., Zou, J., Zeng, B., Rao, J. W. & Xia, K. Non-Hermitian topological magnonics. *Phys. Rep.* **1062**, 1–86. https://doi.org/10.1016/j.physrep.2024.01.006 (2024).
69. Yan, Q. *et al.* Advances and applications on non-Hermitian topological photonics. *Nanophotonics* **12**(13), 2247–2271. https://doi.org/10.1515/nanoph-2022-0775 (2023).
70. Li, A. *et al.* Exceptional points and non-Hermitian photonics at the nanoscale. *Nat. Nanotechnol.* **18**(7), 706–720. https://doi.org/10.1038/s41565-023-01408-0 (2023).
71. Zhao, H. *et al.* Non-Hermitian topological light steering. *Science* **365**(6458), 1163–1166. https://doi.org/10.1126/science.aay1064 (2019).
72. Gu, Z. *et al.* Transient non-Hermitian skin effect. *Nat. Commun.*[SPACE]https://doi.org/10.1038/s41467-022-35448-2 (2022).

Acknowledgements

This work is supported by the Fundamental Research Funds for the Central Universities (Grant No. JUSRP123027), the National Natural Science Foundation of China (Grant No. 12264061), the Zhejiang Provincial Nature Science Foundation under (Grant No. LQ22A040006), and the Science Foundation of Guizhou Science and Technology Department (Grant number QKHJZ[2021]033).

Author contributions

Lei Chen and Zhen-Xia Niu carried out the analytical calculation. Xingran Xu did the numerical simulation and supervised the project.

Competing interests

The authors declare no competing interests.

Additional information

Correspondence and requests for materials should be addressed to X.X.

Reprints and permissions information is available at www.nature.com/reprints.

Publisher's note Springer Nature remains neutral with regard to jurisdictional claims in published maps and institutional affiliations.

Open Access This article is licensed under a Creative Commons Attribution-NonCommercial-NoDerivatives 4.0 International License, which permits any non-commercial use, sharing, distribution and reproduction in any medium or format, as long as you give appropriate credit to the original author(s) and the source, provide a link to the Creative Commons licence, and indicate if you modified the licensed material. You do not have permission under this licence to share adapted material derived from this article or parts of it. The images or other third party material in this article are included in the article's Creative Commons licence, unless indicated otherwise in a credit line to the material. If material is not included in the article's Creative Commons licence and your intended use is not permitted by statutory regulation or exceeds the permitted use, you will need to obtain permission directly from the copyright holder. To view a copy of this licence, visit http://creativecommons.org/licenses/by-nc-nd/4.0/.

© The Author(s) 2024